J|A|C|S
ARTICLES
Published on Web 05/05/2006

Hydrogenation of Arenes over Silica-Supported Catalysts That Combine a Grafted Rhodium Complex and Palladium Nanoparticles: Evidence for Substrate Activation on $Rh_{single-site}-Pd_{metal}$ Moieties

Pierluigi Barbaro,[†] Claudio Bianchini,*[,†] Vladimiro Dal Santo,[‡] Andrea Meli,[†] Simonetta Moneti,[†] Rinaldo Psaro,*[,‡] Adriana Scaffidi,[†] Laura Sordelli,[‡] and Francesco Vizza[†]

Contribution from ICCOM-CNR, Area di Ricerca CNR di Firenze, Via Madonna del Piano 10, 50019 Sesto Fiorentino, Firenze, Italy, and ISTM-CNR, Via C. Golgi 19, 20133 Milano, Italy

Received January 12, 2006; E-mail: claudio.bianchini@iccom.cnr.it

Abstract: The complex Rh(cod)(sulfos) (Rh^I; sulfos = $^-O_3S(C_6H_4)CH_2C(CH_2PPh_2)_3$; cod = cycloocta-1,5-diene), either free or supported on silica, does not catalyze the hydrogenation of benzene in either homogeneous or heterogeneous phase. However, when silica contains supported Pd metal nanoparticles (Pd^0/SiO_2), a hybrid catalyst (Rh^I-Pd^0/SiO_2) is formed that hydrogenates benzene 4 times faster than does Pd^0/SiO_2 alone. EXAFS and DRIFT measurements of in situ and ex situ prepared samples, batch catalytic reactions under different conditions, deuterium labeling experiments, and model organometallic studies, taken together, have shown that the rhodium single sites and the palladium nanoparticles cooperate with each other in promoting the hydrogenation of benzene through the formation of a unique entity throughout the catalytic cycle. Besides decreasing the extent of cyclohexa-1,3-diene disproportionation at palladium, the combined action of the two metals activates the arene so as to allow the rhodium sites to enter the catalytic cycle and speed up the overall hydrogenation process by rapidly reducing benzene to cyclohexa-1,3-diene.

Introduction

The capability of the sulfonate group to form robust H-bonds to terminal silanols has been recently exploited to immobilize transition metal complexes over silica.[1−3] This grafting procedure has been successfully employed to heterogenize the rhodium(I) complex Rh(cod)(sulfos) (Rh^I; sulfos = $^-O_3S(C_6H_4)CH_2C(CH_2PPh_2)_3$; cod = cycloocta-1,5-diene), yielding the supported hydrogen-bonded catalyst Rh(cod)(sulfos)/SiO_2 (Rh^I/SiO_2, Scheme 1a).[1d]

If silica already holds supported palladium particles (Pd^0/SiO_2), the hybrid system Rh^I-Pd^0/SiO_2 is formed, containing both rhodium single sites and palladium particles (Scheme 1b), which exhibits unusual properties as a catalyst for the hydrogenation of arenes.[4] In particular, the combined single-site/dispersed-metal catalyst Rh^I-Pd^0/SiO_2 is 4 times more active than Pd^0/SiO_2 for the hydrogenation of benzene or toluene, while Rh^I/SiO_2 is totally inactive. Independent experiments with cyclohexa-1,3-dienes and cyclohexenes showed that cyclohexa-1,3-dienes are more rapidly reduced to cyclohexenes

Scheme 1

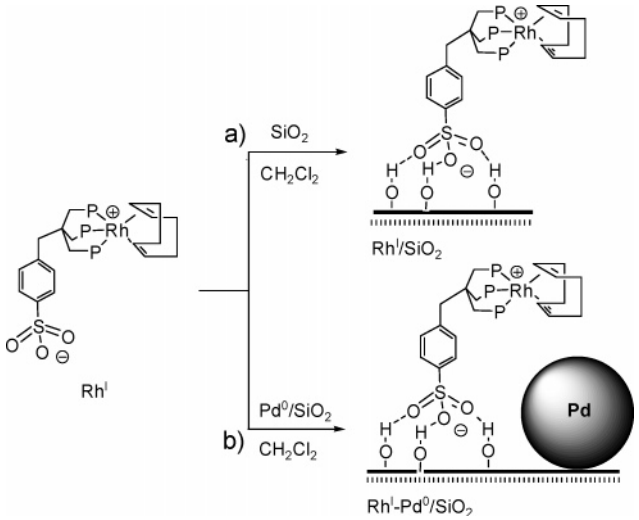

[†] ICCOM-CNR, Sesto Fiorentino, Firenze.
[‡] ISTM-CNR, Milano.

(1) (a) Bianchini, C.; Dal Santo, V.; Meli, A.; Moneti, S.; Moreno, M.; Oberhauser, W.; Psaro, R.; Soredelli, L.; Vizza, F. *J. Catal.* **2003**, *213*, 47. (b) Bianchini, C.; Barbaro, P.; Dal Santo, V.; Gobetto, R.; Meli, A.; Oberhauser, W.; Psaro, R.; Vizza, F. *Adv. Synth. Catal.* **2001**, *343*, 41. (c) Bianchini, C.; Dal Santo, V.; Meli, A.; Oberhauser, W.; Psaro, R.; Vizza, F. *Organometallics* **2000**, *19*, 2433. (d) Bianchini, C.; Burnaby, D. G.; Evans, J.; Frediani, P.; Meli, A.; Oberhauser, W.; Psaro, R.; Sordelli, L.; Vizza, F. *J. Am. Chem. Soc.* **1999**, *121*, 5961.
(2) De Rege, F. M.; Morita, D. K.; Ott, K. C.; Tumas, W.; Broene, R. D. *Chem. Commun.* **2000**, 1797.
(3) (a) Bianchini, C.; Meli, A.; Vizza, F. In *The Handbook of Homogeneous Hydrogenation*; de Vries, J. G., Ed.; Wiley-VCH: Weinheim, Germany, 2006. (b) Thomas, J. M.; Raja, R.; Lewis, D. W. *Angew. Chem., Int. Ed.* **2005**, *44*, 6456.
(4) Bianchini, C.; Dal Santo, V.; Meli, A.; Moneti, S.; Moreno, M.; Oberhauser, W.; Psaro, R.; Sordelli, L.; Vizza, F. *Angew. Chem., Int. Ed.* **2003**, *42*, 2636.

Scheme 2

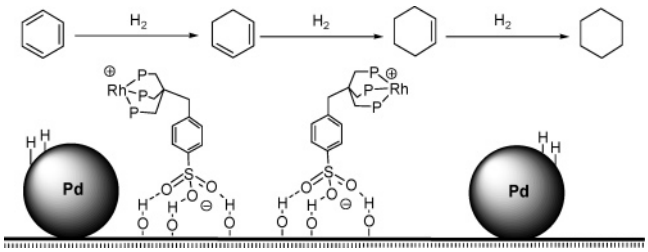

at rhodium, while cyclohexenes are predominantly reduced at palladium. It was also found that the cyclohexa-1,3-diene disproportionation, occurring on palladium, is inhibited by the grafted rhodium complex. On the basis of these pieces of information as well as a number of experiments, including the isolation of relevant intermediates, the authors concluded that the enhanced activity of the $Rh^{I}-Pd^{0}/SiO_2$ catalyst is due not to hydrogen spillover,[5] as suggested by other authors for arene hydrogenation by tethered complexes on supported metals (TCSM),[6] but to the fact that the rate-limiting hydrogenation of benzenes to cyclohexa-1,3-dienes is assisted by both palladium and rhodium. The concerted action of the two metals, besides preventing the competitive diene disproportionation to benzene and cyclohexene, apparently speeds up the reduction of the first double bond (Scheme 2). However, it was concluded that *the intimate* mechanism of the Pd−Rh interaction in the first hydrogenation step is still rather obscure.[4] Addressing this question would be of importance, as it would open the door to the rational design of a new generation of tailored heterogeneous catalysts for diverse applications through appropriate combinations of supported metals and grafted molecular complexes. Indeed, several TCSM catalysts, with either covalent or H-bond grafting, are actually available with proven effectiveness in a variety of processes such as arene hydrogenation,[5,6] enantioselective hydrogenation of alkenes,[1b,2] hydrodefluorination of fluoroarenes,[7] alkene hydroformylation,[1d,8] hydrodechlorination of chlorophenols,[5,9] and hydrogenolysis of benzylic functions.[10]

In an attempt at elucidating the synergic action exerted by rhodium and palladium on arene hydrogenation, an extended X-ray absorption fine structure (EXAFS) study has been carried out on several catalytically relevant or model compounds, including the starting precursor $Rh^{I}-Pd^{0}/SiO_2$, before and after hydrogenation, and the termination metal product of a batch hydrogenation of benzene. Parallel to the EXAFS investigation, all relevant materials were characterized by high-resolution transmission electron microscopy (HRTEM), and the hydrogenation of benzene and toluene was achieved under different catalytic conditions to draw out experimental kinetic information. In this paper is reported an account of this multiform study, which we feel has substantially contributed to shed light on the intimate mechanism of the palladium−rhodium interaction.

Experimental Section

General Information. All reactions and manipulations were routinely performed under a nitrogen or argon atmosphere by using standard Schlenk techniques, unless stated otherwise. CH_2Cl_2 and *n*-pentane were distilled under nitrogen from CaH_2 and $LiAlH_4$, respectively. Benzene and toluene employed in the catalytic reactions were distilled over Na prior to use. The rhodium complex Rh(cod)-(sulfos) (Rh^{I}) was prepared as previously described.[11] All the other reagents and chemicals were reagent grade and were used as received from commercial suppliers. The Davicat (Grace) silica employed in this work was a high-surface-area hydrophilic mesoporous nonordered material. The support was ground, washed with 1 M HNO_3 and distilled water to neutrality, and dried overnight in an oven at 100 °C. Porosimetry and surface area were determined by nitrogen adsorption. Nitrogen adsorption/desorption isotherms at liquid nitrogen temperature were measured on a Micromeritics ASAP 2010 instrument. All silica samples were routinely pre-outgassed at 300 °C. Average pore radius (9.70 nm) and specific pore volume (1.43 cm^3/g) were calculated according to the Barret−Joyner−Halenda (BJH) theory.[12] The specific surface area (295 m^2/g) was obtained using the Brunauer−Emmett−Teller (BET) equation.[13] The rhodium contents in the tethered catalysts were determined by inductively coupled plasma atomic emission spectroscopy (ICP-AES) with a Jobin Yvon (series JY24) instrument at a sensitivity level of 500 ppb. Each sample (20−50 mg) was treated in a microwave-heated digestion bomb (Milestone, MLS-200) with concentrated HNO_3 (1.5 mL), 98% H_2SO_4 (2 mL), 37% HCl (0.5 mL), and a pellet (0.4 g) of a digestion aid reagent (0.1% Se in K_2SO_4). After the silica particles were filtered off, the solutions were analyzed. The addition of selenium was necessary to get an effective digestion of the phosphine ligand, which was hardly achievable by usual acid dissolution procedures. The same digestion method was employed to determine the metal contents in the products recovered after catalysis and in the organic solutions. The palladium contents in the heterogeneous catalysts were determined by flame atomic absorption spectroscopy (AAS) with a Perkin-Elmer 400 atomic absorption spectrophotometer. Each sample (ca. 50 mg) was treated with aqua regia (ca. 12 mL) and then heated to the boiling temperature for 1−2 h, during which time two 3-mL portions of HCl were added to the mixture. Batch reactions under a controlled pressure of gas were performed with a stainless steel Parr 4565 reactor (100 mL) equipped with a Parr 4842 temperature and pressure controller and a paddle stirrer. GC analyses of the solutions were performed on a Shimadzu GC-14 A gas chromatograph equipped with a flame ionization detector and a 30 m (0.25 mm i.d., 0.25 μm film thickness) SPB-1 Supelco fused silica capillary column. GC/MS analyses were performed on a Shimadzu QP 5000 apparatus equipped with an identical capillary column. The stereochemistry of the benzene hydrogenation product was investigated by $^{13}C\{^1H\}$ NMR spectroscopy using 99.9% deuterated C_6D_6. $^{13}C\{^1H\}$ NMR spectra were recorded on a Bruker Avance DRX-400 spectrometer operating at 100.613 MHz and equipped with a temperature controller accurate to ±0.1 °C. A total of 2048 scans of size 64K covering the full range (15 432.1 Hz) were acquired with a relaxation delay of 5 s. Chemical shifts are relative to external TMS, with downfield values reported as positive. Experimental $^{13}C\{^1H\}$ NMR spectra were computer simulated using the gNMR program.[14] Diffuse reflectance infrared Fourier transform (DRIFT) spectra were recorded on a Digilab FTS-60 instrument, equipped with a KBr beam-splitter,

(5) Abu-Reziq, R.; Avnir, D.; Miloslavski, I.; Schumann, H.; Blum, J. *J. Mol. Catal. A: Chem.* **2002**, *185*, 179.
(6) (a) Stanger, K. J.; Tang, Y.; Anderegg, J.; Angelici, R. J. *J. Mol. Catal. A: Chem.* **2003**, *202*, 147. (b) Yang, H.; Gao, H.; Angelici, R. J. *Organometallics* **2000**, *19*, 622. (c) Gao, H.; Angelici, R. J. *Organometallics* **1999**, *18*, 989. (d) Gao, H.; Angelici, R. J. *J. Mol. Catal. A: Chem.* **1999**, *145*, 83. (e) Perera, M. A. D. N.; Angelici, R. J. *J. Mol. Catal. A: Chem.* **1999**, *149*, 99. (f) Gao, H.; Angelici, R. J. *New J. Chem.* **1999**, *23*, 633. (g) Gao, H.; Angelici, R. J. *J. Am. Chem. Soc.* **1997**, *119*, 6937.
(7) Yang, H.; Gao, H.; Angelici, R. J. *Organometallics* **1999**, *18*, 2285.
(8) Gao, H.; Angelici, R. J. *Organometallics* **1998**, *17*, 3063.
(9) (a) Bovkun, T. T.; Sasson, Y.; Blum, J. *J. Mol. Catal. A: Chem.* **2005**, *242*, 68. (b) Ghattas, A.; Abu-Reziq, R.; Avnir, D.; Blum, J. *Green Chem.* **2003**, *5*, 40.
(10) Abu-Reziq, R.; Avnir, D.; Blum, J. *J. Mol. Catal. A: Chem.* **2002**, *187*, 277.
(11) Bianchini, C.; Frediani, P.; Sernau, V. *Organometallics* **1995**, *14*, 5458.
(12) Barrett, E. P.; Joyner, L. G.; Halenda, P. P. *J. Am. Chem. Soc.* **1951**, *73*, 373.
(13) Brunauer, S.; Emmett, P. H.; Teller, E. *J. Am. Chem. Soc.* **1938**, *60*, 309.
(14) Budzelaar, P. H. M. *gNMR V4.0*; Cherwell Scientific Publishing: Oxford, 1995−1997 (Ivory Soft).

using a homemade reaction chamber with ZnSe windows and an Harrick DRA-2C1 accessory.[15] HRTEM micrographs were recorded on a JEOL 200EX instrument. Pd^{0}/SiO_2, usually 1 g batches (Pd content ranging from 1.99 to 9.85 wt %),[4] and Rh^{I}/SiO_2 (rhodium content from 0.3 to 1.7 wt %)[1d] were prepared following previously reported procedures. Details of syntheses and acquisition of DRIFT spectra and HRTEM micrographs are given as Supporting Information.

Preparation of $Rh^{I}-Pd^{0}/SiO_2$. The samples of this bimetallic catalyst (0.26−1.35 wt % Rh and 1.99−9.85 wt % Pd) were prepared following a procedure analogous to that reported above for the silica-tethered rhodium(I) complex Rh^{I}/SiO_2 using as support material, instead of the pretreated silica, Pd^{0}/SiO_2 (Pd content ranging from 1.99 to 9.85 wt %), previously passivated under O_2 flow (40 mL/min) for 30 min followed by flushing in argon flow (40 mL/min) for 30 min.[4] The mild passivation of Pd^{0}/SiO_2 is a necessary step to allow for the grafting of Rh(cod)(sulfos), as it takes place in the potentially reactive solvent CH_2Cl_2.[16] However, this does not represent a limitation to catalysis, as the thin oxide layer is rapidly and completely removed under hydrogenation conditions (in situ EXAFS evidence).

Preparation of Pd^{0}/NaY. Zeolite (NaY)-supported palladium nanoparticles (Pd^{0}/NaY), usually 1 g batches (ca. 2 wt % Pd), were obtained by ionic exchange of NaY with $Pd(NH_3)_4(NO_3)_2$ followed by (1) calcination at 250 °C for 2 h in O_2 flow (40 mL/min) at a heating rate of 1 °C/min, followed by cooling in argon flow (40 mL/min) to room temperature; (2) reduction at 300 °C for 1 h in H_2 flow (40 mL/min) at a heating rate of 10 °C/min followed by cooling in argon flow (40 mL/min) to room temperature. Ionic exchange was performed as follows: 5 g of NaY was treated with 100 mL of a 0.01 M solution of $Pd(NH_3)_4(NO_3)_2$ and stirred overnight at 70 °C. The suspension was filtered, thoroughly washed, and dried overnight at 100 °C.

Preparation of $Rh^{I}-Pd^{0}$/ NaY. This bimetallic catalyst was prepared following a procedure analogous to that reported above for $Rh^{I}-Pd^{0}/SiO_2$, using as support material Pd^{0}/NaY (ca. 2 wt % Pd), previously passivated under O_2 flow (40 mL/min) for 30 min followed by flushing in argon flow (40 mL/min) for 30 min.

EXAFS Experiments. EXAFS experiments were conducted at the EXAFS XAS13 beamline of the DCI synchrotron of LURE at Orsay, with a double-crystal Ge(400) monochromator. The spectra were recorded in transmission at the Pd K-edge and in fluorescence at the Rh K-edge. The samples were loaded inside the sample holders under a nitrogen atmosphere and measured at room temperature over a range of 1000 eV after the edge, with a sampling step of 2 eV and 2−4 s integration per point. Each spectrum was repeated three or four times for the signal-to-noise ratio optimization and for the error bars evaluation. Pd and Rh foils were employed as reference standards for the extraction of phase and amplitude experimental functions. The single scattering data analysis, used in the signal modeling at the Pd K-edge, was performed with the software package of A. Michalowicz. Experimental $\chi(k)$ functions were extracted from the absorption spectra with a standard procedure and Fourier transformed over a k range of 3−15 $Å^{-1}$. The main peaks of the Fourier transformed modulus were filtered and analyzed with a nonlinear least-squares fit program which provides the atomic species, the number N of nearest neighbors, their distance R from the absorber atom, and the disorder factor σ_{DW} for each shell. The analysis at the Rh K-edge was performed also by including the simulation of the multiple scattering contributions present in the signals. For this analysis the FEFF7 program package was used[17] which calculates, starting from a model structure, all the theoretical signals produced by all the single and multiple scattering paths.

The fits were performed on the unfiltered k^3-weighted spectra. Scattering paths were included up to the distance of 4.5 Å, because no signal was detectable in the FFT of any samples beyond $r = 4$ Å. Paths with relative amplitude lower than 6% were neglected. The Rh and Pd K-edge Fourier transform spectra (not phase corrected) are reported in Figures 1−4. The best-fit values determined for the structural parameters of each shell of every sample are reported in Tables 1−3.

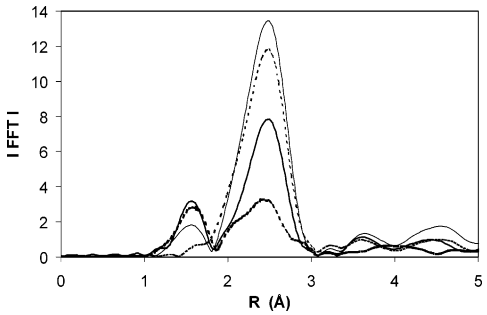

Figure 1. Pd K-edge Fourier spectra (not phase-corrected) of (bold —) Pd^{0}/SiO_2, 1.99 wt % Pd; (—) Pd^{0}/SiO_2, 9.85 wt % Pd; (bold ···) $Rh^{I}-Pd^{0}/SiO_2$, 0.54−1.99 wt % Rh−Pd; (···) $Rh^{I}-Pd^{0}/SiO_2$, 0.46−9.85 wt % Rh−Pd.

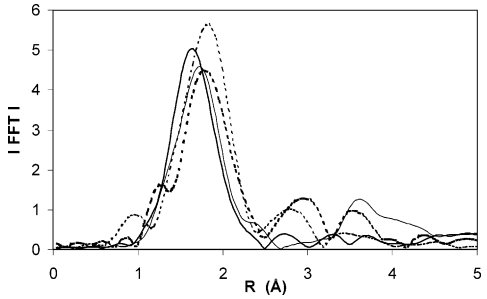

Figure 2. Rh K-edge Fourier spectra (not phase-corrected) of (···) Rh^{I}; (bold ···) Rh^{I}/SiO_2, 0.94 wt % Rh; (bold —) $Rh^{I}-Pd^{0}/SiO_2$, 0.54−1.99 wt % Rh−Pd; (—) $Rh^{I}-Pd^{0}/SiO_2$, 0.46−9.85 wt % Rh−Pd.

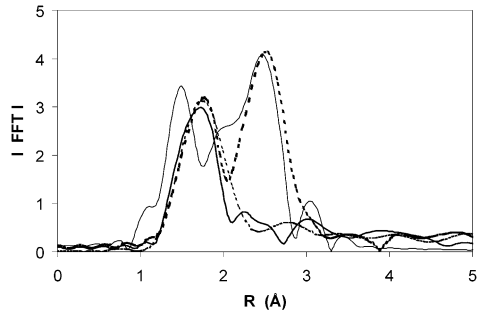

Figure 3. Rh K-edge Fourier spectra (not phase-corrected) of (bold —) Rh^{I}/SiO_2, 0.94 wt % Rh, after in situ reduction with H_2 flow at 130 °C; (bold ···) $Rh^{I}-Pd^{0}/SiO_2$, 0.46−9.85 wt % Rh−Pd, after in situ reduction with H_2 flow at 130 °C; (···) Rh^{I}/SiO_2, 0.94 wt % Rh, after in situ reduction with H_2 flow at 300 °C; (—) $Rh^{I}-Pd^{0}/SiO_2$, 0.46−9.85 wt % Rh−Pd, at the end of a batch reaction of benzene hydrogenation (30 bar, 40 °C).

Heterogeneous Hydrogenation Reactions with $Rh^{I}-Pd^{0}/SiO_2$ as Catalyst. The autoclave was charged with the appropriate amount of a selected sample of $Rh^{I}-Pd^{0}/SiO_2$, the desired amount of benzene or toluene, and *n*-pentane (complement to 30 mL total volume). The ensemble was pressurized with H_2 to the desired pressure, heated to 40 °C, and then stirred at 1500 rpm. After 2 h, the autoclave was cooled to ambient temperature and depressurized. The liquid contents were analyzed by GC and GC/MS. Above 1500 rpm, the rates were independent of the agitation speed at all the temperatures studied, thus indicating the absence of mass transport resistance. For comparative purposes, some hydrogenation reactions were also carried out using either Pd^{0}/SiO_2 or Rh^{I}/SiO_2 or $Rh^{I}-Pd^{0}$/NaY as catalysts. The stability of the immobilized catalyst against leaching from the support was tested by recycling experiments (see Supporting Information).

(15) Dal Santo, V.; Dossi, C.; Fusi, A.; Psaro, R.; Mondelli, C.; Recchia, S. *Talanta* **2005**, *66*, 674.
(16) Solymosi, F.; Rasko, J. *J. Catal.* **1995**, *155*, 74.
(17) (a) Zabinsky, S. I.; Rehr, J. J.; Ankuninov, A.; Albers, R. C.; Eller, M. J. *Phys. Rev. B* **1995**, *52*, 2995. (b) Mustre de Leon, J.; Rehr, J. J.; Zabinsky, S. I.; Albers, R. C. *Phys. Rev. B* **1991**, *44*, 4146.

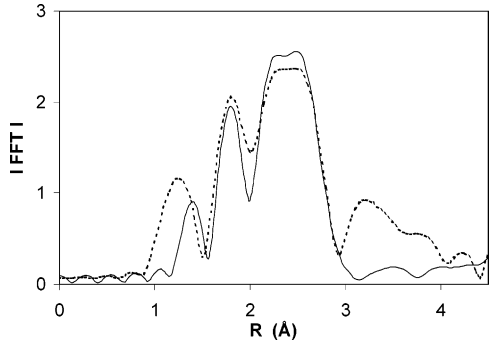

Figure 4. Rh K-edge Fourier spectra (not phase-corrected) of (···) Rh^I-Pd^0/SiO_2, 0.46−9.85 wt % Rh−Pd, exposed to 1 bar CO after reduction in H_2 flow at 130 °C; (—) Rh^I-Pd^0/SiO_2, 0.46−9.85 wt % Rh−Pd, exposed to 5 bar CO after hydrogenation in an autoclave (30 bar, 40°C).

Table 1. Best-Fit EXAFS Data at the Pd K-Edge

sample	shell	*N*	*r* (Å)	σ_{DW} ($\times 10^{-2}$ Å)
Pd^0/SiO_2 (1.99 wt % Pd)	O	2.5 ± 0.5	1.98 ± 0.01	9.7 ± 0.4
	Pd	5.8 ± 0.6	2.70 ± 0.006	8.8 ± 0.5
Pd^0/SiO_2 (9.85 wt % Pd)	O	1.3 ± 0.2	1.97 ± 0.01	9.2 ± 0.2
	Pd	7.8 ± 0.3	2.74 ± 0.002	7.9 ± 0.1
Rh^I-Pd^0/SiO_2	O	2.5 ± 0.4	1.98 ± 0.01	9.9 ± 0.3
(0.54−1.99 wt % Rh−Pd)	Pd	4.8 ± 0.8	2.70 ± 0.01	9.9 ± 0.1
Rh^I-Pd^0/SiO_2	Pd	9.0 ± 0.1	2.70 ± 0.003	8.8 ± 0.1
(0.46−9.85 wt % Rh−Pd)				

Preparation of Samples for EXAFS Measurements. Hydrogenation Reactions in an Autoclave. (A) With No Substrate. A 100 mL Parr autoclave was charged with 47 mg of Rh^I-Pd^0/SiO_2 (0.46−9.85 wt % Rh−Pd) and *n*-pentane (30 mL). The ensemble was pressurized with H_2 to 30 bar, heated to 40 °C, and then stirred (1500 rpm). After 2 h, the autoclave was cooled to ambient temperature and depressurized. The solid residue was separated by filtration over a sintered glass from the liquid phase and washed with *n*-pentane (3 × 20 mL) under a hydrogen pressure.

(B) With No Substrate Followed by CO Pressurization. Following a procedure analogous to that reported above, after the hydrogenation phase, the autoclave was cooled to ambient temperature, depressurized, and then pressurized to 5 bar with CO. After 30 min, the autoclave was depressurized, and the solid residue was filtered off and washed with *n*-pentane (3 × 20 mL) under CO.

(C) With Benzene as Substrate. The autoclave was charged with 47 mg of Rh^I-Pd^0/SiO_2 (0.46−9.85 wt % Rh−Pd) and a solution of 0.43 mL (4.81 mmol) of benzene in *n*-pentane (complement to 30 mL total volume). The ensemble was pressurized with H_2 to 30 bar, heated to 40 °C, and then stirred (1500 rpm). After 2 h, the autoclave was cooled to ambient temperature and depressurized. The liquid contents were analyzed by GC and GC/MS. The grafted rhodium/palladium product was separated by filtration over a sintered glass from the liquid phase under nitrogen and washed with *n*-pentane (3 × 20 mL).

Results and Discussion

EXAFS and HRTEM Characterization of Pd^0/SiO_2, Rh^I/SiO_2, and Rh^I-Pd^0/SiO_2. An EXAFS analysis of Pd^0/SiO_2 (1.99 wt % Pd) at the Pd K-edge showed a Pd−Pd nearest-neighbors value (N_{Pd-Pd}) of 5.8 as well as a peak trend for the next shells, consistent with the formation of small metal particles dispersed on the support (Table 1, Figure 1). An appreciable contribution from the surface oxygen atoms ($N_{Pd-O} = 2.5$) was also observed. As the palladium foil has a fcc crystal frame with 12 nearest neighbors at 2.75 Å, on the assumption of particles growth with the same packing and cubooctahedric geometry, a mean diameter of about 10 Å was calculated for the palladium particles.

In Pd^0/SiO_2 (9.85 wt % Pd), the metal particles were still small enough to exhibit a contribution from the surface oxygen ($N_{Pd-O} = 1.3$), but with a larger Pd−Pd nearest-neighbors value ($N_{Pd-Pd} = 7.8$) as compared to the 1.99 wt % sample, corresponding to an estimated mean diameter of 13 Å (Table 1).

An EXAFS analysis of Rh^I-Pd^0/SiO_2 (0.46−9.85 wt % Rh−Pd) at the Rh K-edge (Table 2, Figure 2) revealed that all rhodium atoms on the support maintain the coordination environment as in the free complex Rh^I (Table 3, Figure 2), the four C atoms from cod and the three P atoms from the triphosphine ligand being well resolved. An identical coordination geometry about rhodium was observed by EXAFS for the mixed-metal system Rh^I-Pd^0/SiO_2 (0.54−1.99 wt % Rh−Pd) (Table 2, Figure 2) as well as for Rh^I/SiO_2 (0.94 wt % Rh) (Table 3, Figure 2).

Irrespective of the metal loading in Rh^I-Pd^0/SiO_2, contributions due to Pd−Rh couples were not observed at the Rh K-edge (Table 2, Figure 2), while rinsing the hybrid complex with neat MeOH-d_4 gave a solution of Rh^I (NMR evidence), which is consistent with the integrity of the grafted molecular rhodium complex.[1d]

On the basis of the EXAFS data, one may therefore conclude that Rh^I is anchored intact on the silica surface irrespective of the palladium loading with no evidence of Pd−Rh interaction.

The Pd^0 metal particle mean diameter measured by HRTEM (Table 4) on Pd^0/SiO_2 (1.99 wt % Pd) was 18.3 Å. Metal particles were visible both on the surface and on the edges of the support grains that were totally amorphous. The particle distribution function was sharp and symmetric, but the distribution through the different support grains was not homogeneous. The morphology and dispersion of the palladium particles, with a mean diameter of 20.5 Å, were almost unchanged in Pd^0/SiO_2 (9.85 wt % Pd) as compared to the 1.99 wt % sample, while the total number of particles on the surface was apparently higher.

A large-spot (50 nm) energy-dispersive spectrometry (EDS) analysis on Rh^I-Pd^0/SiO_2 (1.08−1.99 wt % Rh−Pd) showed the emission peaks of rhodium and palladium to be consistent with a Pd/Rh molar ratio of 2 over the areas where the palladium particles were visible by TEM (in perfect agreement with the overall metal loading). When a region without visible metal aggregates was shot, the EDS still detected both metals but in a Pd/Rh molar ratio <1. Taking into account the molar weight of rhodium, palladium, and SiO_2, Rh−Pd loadings of 1.08−1.99 wt % correspond to molar fractions of about 0.005 and 0.010, respectively, which is at the limit of the EDS sensitivity. However, when small probe areas were selected around the palladium particles, the molar fraction of supported Pd atoms per volume unit could be increased so as to detect the contribution from either metal. In this way, operating with an electron probe spot of 5 nm centered on a single metal particle (17 Å diameter), a molar ratio could be estimated. In particular, since in fcc packing a palladium particle with a diameter of 17 Å has a surface atoms/total atoms ratio of 70%, a Pd/Rh value of 10 corresponds to an average of one rhodium atom every seven surface palladium atoms.

Table 2. Best-Fit EXAFS Data at the Rh K-Edge for Bimetallic Samples

sample	shell	*N*	*r* (Å)	σ_{DW} ($\times 10^{-2}$ Å)
$Rh^{I}-Pd^{0}/SiO_2$ (0.54−1.99 wt % Rh−Pd)	C	4.0 ± 0.2	2.19 ± 0.02	8.1 ± 0.5
	P	3.0 ± 0.2	2.40 ± 0.01	9.3 ± 0.5
$Rh^{I}-Pd^{0}/SiO_2$ (0.46−9.85 wt % Rh−Pd)	C	4.0 ± 0.2	2.19 ± 0.03	8.1 ± 0.5
	P	3.0 ± 0.2	2.41 ± 0.02	9.3 ± 0.5
$Rh(H)_x-Pd/SiO_2$ obtained by in situ reduction of $Rh^{I}-Pd^{0}/SiO_2$ (0.46−9.85 wt % Rh−Pd) with H_2 flow at 130 °C	P	3.0 ± 0.2	2.32 ± 0.02	9.3 ± 0.5
	Pd	3.4 ± 0.2	2.77 ± 0.03	9.8 ± 0.5
$Rh(H)_x(CO)_y-Pd(CO)_x/SiO_2$ obtained by in situ reduction of $Rh^{I}-Pd^{0}/SiO_2$ (0.46−9.85 wt % Rh−Pd) with H_2 flow at 130 °C, followed by CO addition	C	1.4 ± 0.2	1.91 ± 0.01	9.9 ± 0.5
	P	2.0 ± 0.2	2.34 ± 0.01	9.3 ± 0.5
	O_b	0.9 ± 0.2	2.62 ± 0.03	5.8 ± 0.5
	O_l	0.6 ± 0.2	2.92 ± 0.03	4.2 ± 0.5
	Pd	2.1 ± 0.2	2.77 ± 0.02	9.9 ± 0.5
$Rh(H)_x(CO)_y-Pd(CO)_x/SiO_2$ obtained by reduction of $Rh^{I}-Pd^{0}/SiO_2$ (0.46−9.85 wt % Rh−Pd) with H_2 (30 bar) at 40 °C in an autoclave followed by CO (5 bar)	C	1.4 ± 0.2	1.90 ± 0.04	9.9 ± 0.5
	P	2.1 ± 0.2	2.31 ± 0.04	9.9 ± 0.5
	O_b	1.0 ± 0.2	2.61 ± 0.02	6.2 ± 0.5
	O_l	0.4 ± 0.2	2.93 ± 0.03	5.1 ± 0.5
	Pd	1.8 ± 0.2	2.77 ± 0.03	9.1 ± 0.5
solid product obtained after catalytic hydrogenation (30 bar H_2) of benzene with $Rh^{I}-Pd^{0}/SiO_2$ (0.46−9.85 wt % Rh−Pd) at 40 °C in an autoclave	C	4.0 ± 0.2	2.08 ± 0.02	11.0 ± 0.5
	P	1.6 ± 0.2	2.38 ± 0.02	9.7 ± 0.5
	Pd	2.6 ± 0.2	2.76 ± 0.03	8.9 ± 0.5

Table 3. Best-Fit EXAFS Data at the Rh K-Edge for Monometallic Samples

sample	shell	*N*	*r* (Å)	σ_{DW} ($\times 10^{-2}$ Å)
Rh^{I}	C	4.1 ± 0.4	2.19 ± 0.01	9.1 ± 0.6
	P	3.2 ± 0.3	2.49 ± 0.01	9.0 ± 0.8
Rh^{I}/SiO_2 (0.94 wt % Rh)	C	4.0 ± 0.4	2.20 ± 0.01	6.2 ± 0.5
	P	2.8 ± 0.1	2.43 ± 0.01	9.3 ± 0.9
$Rh(H)_x/SiO_2$ obtained by in situ reduction of Rh^{I}/SiO_2 (0.94 wt % Rh) with H_2 flow at 130 °C	P	3.0 ± 0.2	2.27 ± 0.01	9.9 ± 0.6
$Rh(H)_x/SiO_2$ obtained by in situ reduction of Rh^{I}/SiO_2 (0.94 wt % Rh) with H_2 flow at 300 °C	P	3.0 ± 0.2	2.27 ± 0.01	9.9 ± 0.6

Table 4. Mean Diameters of the Pd^{0} Particles by HRTEM and Calculated by EXAFS

	d_{mean} (Å)	
sample	HRTEM	EXAFS
Pd^{0}/SiO_2 (1.99 wt %)	18.3 ± 1.9	10
Pd^{0}/SiO_2 (9.85 wt %)	20.5 ± 1.5	13
$Rh^{I}-Pd^{0}SiO_2$ (0.54−1.99 wt % Rh−Pd)	15.5 ± 1.1	8
$Rh^{I}-Pd^{0}/SiO_2$ (1.08−1.99 wt % Rh−Pd)	13.7 ± 2.5	
$Rh^{I}-Pd^{0}/SiO_2$ (0.46−9.85 wt % Rh−Pd)	20.6 ± 2.0	18
Pd^{0}/NaY (2.01 wt %)	11.8 ± 0.7	
$Rh^{I}-Pd^{0}$NaY (0.15−2.01 wt % Rh−Pd)	16.5 ± 1.3	

In $Rh^{I}-Pd^{0}/SiO_2$ (0.54−1.99 wt % Rh−Pd), the particle size distribution was sharp, with a mean diameter of 15.5 Å (Table 4). No rhodium contribution was detected in the EDS signal, even when the electron beam (5 nm spot) was focused on a single Pd particle, which means that the rhodium molar fraction was everywhere lower than the sensitivity limit.

Provided one considers that EXAFS tends to overestimate the contribution of the smallest particles which, in contrast, are generally underestimated by the TEM images, a good agreement has been found between the mean dimensions estimated from the EXAFS Pd−Pd nearest-neighbors numbers and the HRTEM micrographs analysis.

EXAFS Analysis of the Products Obtained by Hydrogenation of Rh^{I}/SiO_2 and $Rh^{I}-Pd^{0}/SiO_2$. Solid−Gas Conditions. Rh^{I}/SiO_2 (0.94 wt % Rh) was treated with a H_2 flow at 130 °C directly in the EXAFS cell (Table 3, Figure 3). An EXAFS analysis showed unambiguously the rhodium atoms to be surrounded by three phosphorus atoms with Rh−P distances slightly shorter than those in the unsupported and supported Rh^{I} complex (Table 3). Since no other atom was seen at a bonding distance, one may conclude that, besides P atoms, the rhodium single sites are very likely surrounded by hydrogen atoms to complete their coordination sphere. In line with a previous study,[1d] the rhodium complex was removed from the silica surface by rinsing with MeOH-d_4, and the product was authenticated by NMR as the binuclear Rh^{III} tetrahydride [RhH-(μ-H)(sulfos)]$_2$. It has been also reported that the homogeneous hydrogenation of [Rh(triphos)(cod)]$^+$ (triphos = $CH_3C(CH_2PPh_2)_3$) leads to the formation of the nonclassical Rh^{III} tetrahydride [Rh(H)$_2$(H$_2$)(triphos)]$^+$, which is unstable in both the solid state and solution unless protected by a hydrogen atmosphere, in the absence of which it spontaneously loses H_2, converting to the tetrahydride [RhH(μ-H)(triphos)]$_2^{2+}$.[18] It is therefore possible that the hydrogenation of Rh^{I}/SiO_2 follows an identical path, leading to the formation of a silica-anchored Rh^{III} polyhydride, hereafter referred to as $Rh(H)_x/SiO_2$, which may contain both classical and nonclassical hydride ligands (Scheme 3).

In the case of the hybrid system $Rh^{I}-Pd^{0}/SiO_2$ (0.46−9.85 wt % Rh−Pd), after reduction with H_2 at 130 °C in the EXAFS cell, besides appreciable contraction of the average Rh−P distance, a relevant contribution from a palladium shell was also detected (N_{Rh-Pd} = 3.4). Apparently, this contribution originates from surface atoms of the palladium particles dispersed on the support (Table 2, Figure 3). In principle, it is not possible to discriminate palladium from rhodium on the basis of photoelectron scatterer, but the attribution of the Rh metal shell to palladium neighbors was unambiguously supported by the evidence that Rh^{I}/SiO_2 did not exhibit any Rh−Rh contribution, even upon treatment with H_2 up to 300 °C (Table 3, Figure 3).

The Rh−Pd distance of 2.77 Å, only slightly longer than that of a Rh−Pd alloy (2.72 Å), and the number of the Rh−Pd

(18) Bakhmutov, V. I.; Bianchini, C.; Peruzzini, M.; Vizza, F.; Vorontsov, E. V. *Inorg. Chem.* **2000**, *38*, 1655.

Scheme 3

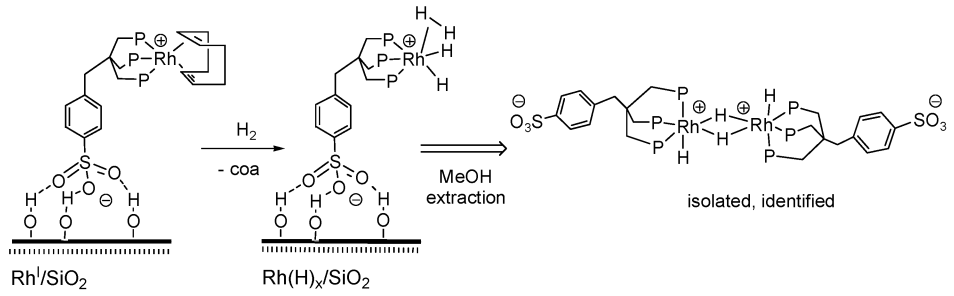

Scheme 4

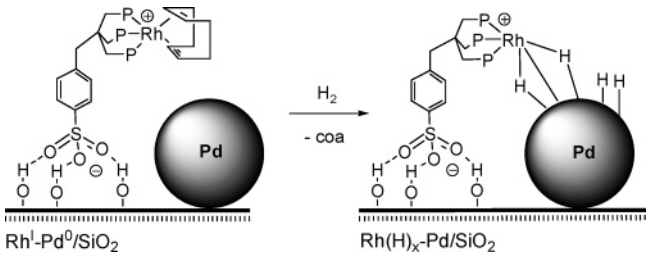

neighbors (3.4) point to rhodium and palladium atoms in close proximity. Metal−metal bonds are frequently encountered in organometallic and coordination compounds, where hydride ligands bridge metal centers. Unfortunately, we did not find evidence in the literature for bimetallic complexes containing Rh(μ-H)$_x$Pd moieties, yet several compounds are known where the Rh(triphos) fragment is connected to other metal fragments (M = Fe, Co, Ni, Rh) by double and triple hydride bridges to give binuclear complexes containing short metal−metal bonds.[19] On the basis of the EXAFS measurements and of previous reports on the homogeneous hydrogenation of Rh-triphos and Rh-sulfos complexes, showing the formation of Rh(μ-H)$_x$Rh binuclear species with metal−metal bonds,[20] we suggest that Rh^I−Pd^0/SiO$_2$ reacts with H_2 to give new surface species where the rhodium single sites and the palladium particles are connected by Rh−Pd bonds as well as bridging hydrides (Scheme 4). This product is hereafter denoted as Rh(H)$_x$−Pd/SiO$_2$.

Solid−Liquid Conditions. Since the catalytic hydrogenation of arenes investigated in this work was carried out in solid−liquid conditions, attempts were made at studying the product arising from the hydrogenation of Rh^I−Pd^0/SiO$_2$ in *n*-pentane in an autoclave (30 bar H_2, 40 °C). Unfortunately, all our efforts to intercept and characterize Rh(H)$_x$−Pd/SiO$_2$ from a solid−liquid reaction were unsuccessful due to the extreme sensitivity to oxygen of the isolated product. Moreover, treatment of the latter with MeOH, even under a H_2 atmosphere, did not allow us to extract a well-defined rhodium-sulfos complex as occurs either for Rh(H)$_x$/SiO$_2$ (see above) or for Rh(CO)$_2$(sulfos)/SiO$_2$.[1d,4] Actually, most of rhodium remained grafted to the silica surface, and extraction with MeOH gave only a tiny amount of an intractable material, containing palladium metal, phosphine oxide, and unknown rhodium-sulfos species (NMR, IR, ICP-AES). We therefore concluded that the hydrogenation of Rh^I−Pd^0/SiO$_2$ in *n*-pentane gives a product in which the Rh−Pd interaction is strong enough to persist after treatment with a polar solvent such as MeOH that it is known to break the H-bonding interaction between sulfos and silica.

In an attempt at stabilizing the hydrogenation product of Rh^I−Pd^0/SiO$_2$, a sample with 0.46−9.85 wt % Rh−Pd was hydrogenated in *n*-pentane in an autoclave (30 bar H_2, 40 °C). CO (5 bar) was then admitted into the reactor. The isolated product was studied by EXAFS. For comparative purposes, an EXAFS study was carried out also on the carbonylation product of Rh(H)$_x$−Pd/SiO$_2$, prepared in solid−gas conditions in the EXAFS cell as previously described (Table 2). Multiple scattering was employed for the carbonyl groups, with a bond angle of 180° between the carbon and oxygen atoms.

The spectra of the two products were extremely similar to each other, which indicates an identical reaction path in either phase system. The corresponding fits (Table 2, Figure 4) show that, in either system, the rhodium atom is coordinated by two phosphorus atoms and two palladium atoms (R_{Rh-P} = 2.34 Å; R_{Rh-Pd} = 2.77 Å). Each rhodium atom is also bonded to an average of 1.4 CO groups (R_{Rh-C} = 1.91 Å, R_{Rh-Ob} = 2.62 Å, R_{Rh-Ol} = 2.92 Å), yet the multiple scattering path contribution from linear carbonyls corresponds to about 40% and 25% of the total carbonyls in the molecule, respectively.

The fact that only two phosphorus atoms are detected in the rhodium coordination sphere suggests that, on the average, one of the sulfos arm is free, which has several precedents in the literature for tripodal triphosphine ligands.[20f,21,22] Moreover, the presence of only 1.4 carbonyl groups and the contribution still relevant from the palladium shell at 2.77 Å show that the interaction between rhodium and palladium, which originated during the hydrogenation process, is not removed by carbonylation (in contrast to what happens to the cod ligand, which is completely removed by CO from Rh^I/SiO$_2$ at room temperature).[1d]

Some possible structures for the hydrogenation/carbonylation product of Rh^I−Pd^0/SiO$_2$ (see also the IR study reported in the following section), hereafter denoted as Rh(H)$_x$(CO)$_y$−Pd(CO)$_x$/SiO$_2$, are reported in Scheme 5.

(19) (a) Bianchini, C.; Laschi, F.; Masi, M.; Mealli, C.; Meli, A.; Ottaviani, M. F.; Proserpio, D. M.; Sabat, M.; Zanello, P. *Inorg. Chem.* **1989**, *28*, 2552. (b) Bianchini, C.; Meli, A.; Laschi, F.; Ramirez, J. A.; Zanello, P.; Vacca, A. *Inorg. Chem.* **1988**, *27*, 4429. (c) Bianchini, C.; Meli, A.; Zanello, P. *Chem. Commun.* **1986**, 628. (d) Bianchini, C.; Mealli, C.; Meli, A.; Sabat, M. *Chem. Commun.* **1986**, 777.

(20) (a) Barbaro, P.; Bianchini, C.; Meli, A.; Moreno, M.; Vizza, F. *Organometallics* **2002**, *21*, 1430. (b) Bianchini, C.; Barbaro, P.; Macchi, M.; Meli, A.; Vizza, F. *Helv. Chim. Acta* **2001**, *84*, 2895. (c) Bianchini, C.; Meli, A.; Moneti, S.; Oberhauser, W.; Vizza, F.; Herrera, V.; Fuentes, A.; Sanchez-Delgado R. A. *J. Am. Chem. Soc.* **1999**, *121*, 7071. (d) Bianchini, C.; Meli, A.; Moneti, S.; Vizza, F. *Organometallics* **1998**, *17*, 2636. (e) Bianchini, C.; Meli, A.; Patinec, V.; Sernau, V.; Vizza, F. *J. Am. Chem. Soc.* **1997**, *119*, 4945. (f) Bianchini, C.; Meli, A.; Peruzzini, M.; Vizza, F.; Frediani, P.; Ramirez, J. A. *Organometallics* **1990**, *9*, 226.

(21) Boxwell, C. J.; Dyson, P. J.; Ellis, D. J.; Welton, T. *J. Am. Chem. Soc.* **2002**, *124*, 9334.

(22) Kiss, G.; Horvath, I. *Organometallics* **1991**, *10*, 3798.

Scheme 5

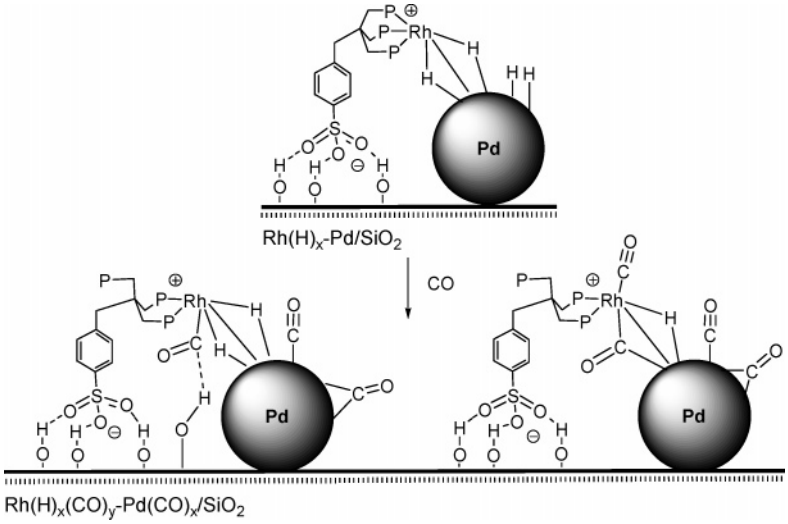

IR Characterization of the Carbonylated Products. Since CO is an excellent IR probe molecule, a DRIFT study has been carried out on significant carbonylation products.

Pd^0/SiO_2 (1.99 and 9.85 wt % Pd), prepared directly in the DRIFT cell by in situ hydrogenation of ex situ calcinated $PdCl_2/SiO_2$, was reacted at room temperature with a flow of 1 bar CO for 30 min. The DRIFT spectra, acquired after the cell was purged with He, are shown in Figure 5.

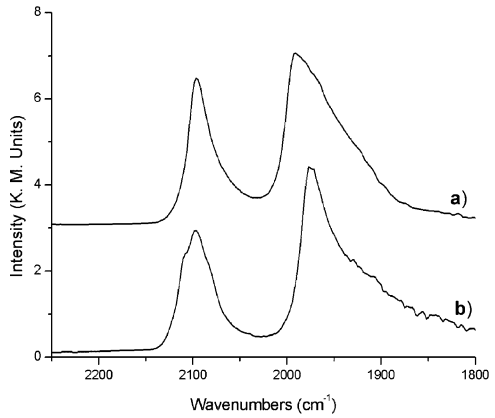

Figure 5. DRIFT spectra of Pd^0/SiO_2 (9.85 wt % Pd, trace a; 1.99 wt % Pd, trace b), after hydrogenation at 120 °C, followed by exposure to 1 bar CO flow for 30 min and purging in He flow for 1 min.

Both samples showed bands located between 2150 and 1900 cm^{-1} due to CO adsorbed on Pd^0 particles. The 1.99 wt % sample showed a band located at 2096 cm^{-1} which is a convolution of three components with maxima at 2108, 2099, and 2080 cm^{-1}. These bands can be attributed to CO adsorbed linearly on different sites of Pd^0 crystallites, while a broad band located at 1977 cm^{-1} may be assigned to bridging CO groups.[23] A band at 2096 cm^{-1} was also present in the spectrum of the 9.85 wt % sample, but the three previous components were less evident, while the broad band attributable to bridging CO was shifted to 1991 cm^{-1}. The intensity ratio of the bands due to bridging and terminal CO has been reported to depend on the metal dispersion.[24] Since quite similar ratios have been found for the samples with 1.99 and 9.85 wt % Pd (2.62 and 2.51, respectively, measured as area $CO_{bridging}$/area CO_{linear}), one may readily conclude that the palladium particles in the two samples exhibit similar dispersion, which is consistent with the HRTEM data.

Samples of Rh^I–Pd^0/SiO_2 (0.54–1.99 wt % Rh–Pd and 0.46–9.85 wt % Rh–Pd) were treated in the DRIFT cell with H_2 at 120 °C and then reacted at room temperature with 1 bar CO. DRIFT spectra, taken after the cell was purged with He, showed a complex system of bands located in the region between 2150 and 1900 cm^{-1} (Figure 6a,b) that may be ascribed to CO bonded both to palladium particles and rhodium single sites. Traces a and b in Figure 6 were well fitted by a superposition of mixed Gaussian/Lorentzian bands, and contributions from different species were put in evidence (fitting bands not showed).

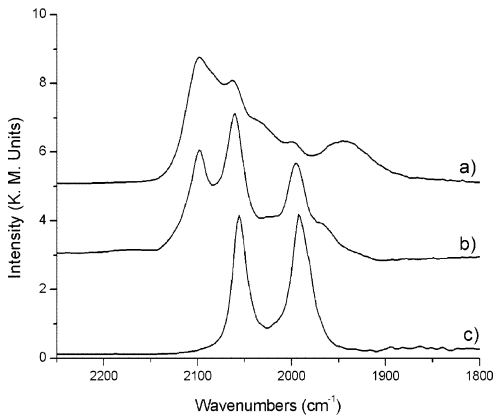

Figure 6. DRIFT spectra of $Rh(H)_x(CO)_y$–$Pd(CO)_x/SiO_2$ after hydrogenation of Rh^I–Pd^0/SiO_2 at 120 °C, followed by exposure at room temperature to 1 bar CO flow for 30 min and purging in He flow for 1 min: (a) 0.54–1.99 wt % Rh–Pd, (b) 0.46–9.85 wt % Rh–Pd. For comparison, the IR spectrum of the sample obtained after hydrogenation/carbonylation of Rh^I/SiO_2 (0.94 wt % Rh) is reported (c).

The bands at 2100 and 1950 cm^{-1} (0.54–1.99 wt % Rh–Pd) and at 2100 and 1968 cm^{-1} (0.46–9.85 wt % Rh–Pd) are attributable to CO bonded to palladium particles in linear and bridging fashion, respectively. However, the for-

(23) Liotta, L. F.; Martin, G. A.; Deganello, G. *J. Catal.* **1996**, *164*, 322 and references therein.

(24) Sheu, L. L.; Sachtler, W. M. H *J. Mol. Catal.* **1993**, *81*, 267 and references therein.

mation of Rh(μ-CO)Pd moieties cannot be excluded. The bands located at 1997 and 2063 cm^{-1} are readily attributable to *gem*-dicarbonyl Rh^I species, as they are present also in the spectra of unsupported[11] and silica-supported $Rh(CO)_2$(sulfos).[1d]

The band at ca. 2030 cm^{-1} has been never observed on freshly hydrogenated/carbonylated samples of Rh^I/SiO_2 (Figure 6c), where only the two bands attributable to *gem*-dicarbonyl Rh^I species are present.[11] Since the EXAFS analysis and the catalytic data led us to exclude the decomposition of the rhodium complex to metallic rhodium particles, this band is not attributable to CO linearly bonded to Rh^0 sites and therefore can be ascribed to a new $Rh-CO_{terminal}$ species. An in-depth inspection of the silanols' O−H stretching bands did not reveal any appreciable variation between spectra recorded under He before and after the treatment with CO.

In conclusion, the DRIFT spectra confirm that the carbonylation of $Rh(H)_x-Pd/SiO_2$ results in a variety of CO bonding modes and also that the hydrogenation of Rh^I-Pd/SiO_2 leads to the formation of surface species where rhodium single sites and palladium particles are interacting with each other.

Zeolite as Support for Rh^I and Pd^0. Palladium nanoparticles were supported on a zeolite NaY material which would prevent the diffusion of the large rhodium complex inside its channels, where the palladium particles are preferentially located. The HRTEM images taken on Pd^0/NaY (2.01 wt %) showed a very narrow particle size distribution function, with a mean value of 11.8 Å (Table 4). All support grains are cubic (with well-resolved channel diffraction fringes of 13 Å) and exhibit a perfectly uniform dispersion of the metal particles. No palladium particles were visible at the external surface of the zeolite, while some palladium particles were visible along the external edge of the zeolite grains.

After impregnation of Pd^0/NaY with Rh^I, HRTEM analysis of the resulting hybrid product Rh^I-Pd^0/NaY (0.15−2.01 wt % Rh−Pd) showed a slightly larger size distribution of the Pd particles (average diameter 16.5 Å) as compared to the sample with no tethered rhodium complex (Table 4). No rhodium contribution was visible in the EDS signal by focusing the electron beam on single Pd particles inside the zeolite, while the emission signal of rhodium was detected on the external surface of the support. This experimental observation is clear evidence that the rhodium complex is preferentially located at the external surface of the zeolite.

EXAFS Analysis after a Batch Hydrogenation of Benzene Catalyzed by Rh^I-Pd^0/SiO_2. A Rh K-edge EXAFS analysis on the product obtained at the end of a batch reaction of benzene hydrogenation catalyzed by Rh^I-Pd^0/SiO_2 (0.46−9.85 wt %) in *n*-pentane (Table 2, Figure 3) showed the presence of four carbon atoms at a distance of 2.08 Å from the rhodium center, which is also connected to 1.6 phosphorus atoms at a distance of 2.38 Å and to 2.6 palladium atoms at a distance of 2.76 Å. This means that the solid product which separates from the catalytic mixture contains rhodium atoms coordinated by a dihapto sulfos ligand and by a C_4 ligand. As previously mentioned, tripodal triphosphines, such as triphos, can act as bidentate ligands, with an unfastened P donor atom, in conjunction with Group 8 and 9 metals, when the coligands occupy more than three coordination positions.[21,22] Since the GC analysis of the liquid phase after catalysis showed the exclusive presence of unreacted benzene and cyclohexane, the C_4 fragment

Scheme 6

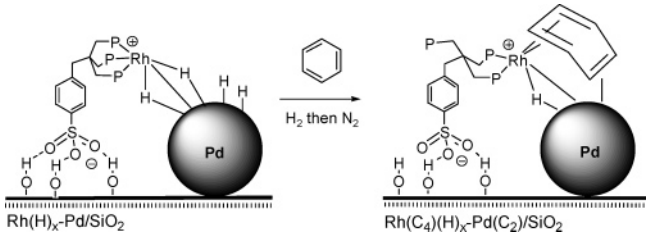

bonded to rhodium may be either the C_4 portion of a benzene molecule or an intermediate species along the reduction of benzene to cyclohexa-1,3-diene.[25] In the former case, it is very likely that the C_2 portion of benzene is bonded to palladium; however, that cannot be proved by EXAFS at the Pd K-edge. On the other hand, Rh^I, either free or immobilized on silica, and its cationic derivative, $[Rh(triphos)(cod)]^+$, are unable to coordinate benzene in any fashion, nor are they able to catalyze benzene hydrogenation to any extent.[4] As it will be discussed below, benzene hydrogenation by late transition metal complexes stabilized by phosphines generally requires the activation of the arene to the η^4 coordination mode,[3a] which is apparently an inaccessible activation path to the $[Rh(triphos)]^+$ fragment.[25] Moreover, hydride(s) transfer from metal to η^4-benzene has been never reported to proceed via a C_4 ligand, allyl-type and ene ligands (η^3) being invariably observed.[25,26] On the basis of this reasoning, which will be further developed in a following section, we propose that the product intercepted at the end of the batch catalytic reaction has the structure shown in Scheme 6, where a benzene molecule is simultaneously activated by palladium and rhodium.

Notably, a Pd K-edge EXAFS analysis on $Rh(C_4)(H)_x-Pd(C_2)/SiO_2$ showed a Pd−Pd coordination number ($N = 9$) coincident with that of the catalyst precursor Rh^I-Pd^0/SiO_2 (see Table 1), which confirms the stability of the palladium particles under hydrogenation conditions.

Benzene and Toluene Hydrogenation Catalyzed by Rh^I-Pd^0/SiO_2 and Rh^I-Pd^0/NaY. All previously reported studies on the hydrogenation of benzene and toluene catalyzed by Rh^I-Pd^0/SiO_2 were carried out with only one type of catalyst (0.56−9.86 wt %) at a H_2 pressure of 30 bar and fixed concentrations of substrate and catalyst amount.[4] To complement the previous data and, most importantly, to obtain information on the reaction mechanism, especially as regards the synergistic cooperation between the rhodium single sites and the palladium particles, we decided to perform a more systematic study where H_2 pressure, substrate concentration, rhodium-to-palladium ratio, and overall catalyst amount are systematically varied.

Tables 5−7 report the data obtained for the hydrogenation of benzene to cyclohexane in the presence of Rh^I-Pd^0/SiO_2, while Table 8 summarizes the results for toluene. Partial hydrogenation products were not detected at any stage of the reactions. All reactions were performed in *n*-pentane at 40 °C. The catalytic activity, in terms of dependence of substrate con-

(25) Bianchini, C.; Caulton, K. G.; Folting, K.; Meli, A.; Peruzzini, M.; Polo, A., Vizza, F. *J. Am. Chem.* Soc. **1992**, *114*, 7290.
(26) (a) Bleeke, J. R.; Muetterties, E. L. *J. Am. Chem. Soc*. **1981**, *103*, 556. (b) Stuhl, L. S.; Rakowski Du Bois, M. C.; Hirsekorn, F. J.; Bleeke, J. R.; Stevens, A. E.; Muetterties, E. L. *J. Am. Chem. Soc*. **1978**, *100*, 2405. (c) Rakowski, M. C.; Hirsekorn, F. J.; Stuhl, L. S.; Muetterties, E. L. *Inorg.* Chem. **1976**, *15*, 2379. (d) Muetterties, E. L.; Hirsekorn, F. J. *J. Am. Chem. Soc*. **1974**, *96*, 4063. (e) Muetterties, E. L.; Hirsekorn, F. J. *J. Am. Chem. Soc*. **1974**, *96*, 7920.

Table 5. Hydrogenation of Benzene to Cyclohexane Catalyzed by $Rh^{I}-Pd^{0}/SiO_2$ (0.46−9.85 wt %): Dependence on Hydrogen Pressure[a]

entry	H_2 pressure (bar)	yield (%);[b] TOF (×10)[c]
1	5	40; 9.62
2	15	42; 10.10
3	30	40; 9.62
4	45	41; 10.10

[a] Experimental conditions: catalyst precursor, 47 mg (Rh, 2.1×10^{-3} mmol; Pd, 43.5×10^{-3} mmol); benzene, 0.43 mL (4.81 mmol); benzene/M ratio, 111 (Pd)−2290 (Rh); *n*-pentane, complement to 30 mL total volume; temperature, 40 °C; time, 2 h; stirring rate, 1500 rpm. [b] Average values over at least three runs. [c] In mmol of product h^{-1}.

version on H_2 pressure, arene concentration, and overall metal amount in the catalyst, was evaluated by using a $Rh^{I}-Pd^{0}/SiO_2$ sample containing ca. 0.5 wt % Rh and ca. 10 wt % Pd. The dependence of substrate conversion on either rhodium or palladium amount in the catalyst precursor was evaluated with $Rh^{I}-Pd^{0}/SiO_2$ samples containing from 0.26 to 1.35 wt % Rh and from 1.99 to 4.87 wt % Pd.

From a perusal of the data obtained by varying the H_2 pressure (Table 5), one may readily infer that the hydrogenation of benzene is zero-order in hydrogen concentration in the pressure range from 5 to 45 bar. A plot of the turnover frequency (TOF) vs substrate concentration showed instead a linear correlation for benzene concentrations lower than 1 M (Table 6, Figure 7). For higher substrate concentrations, a saturation effect apparently occurred, indicated by a plateau in activity.

The TOF tended to a plateau also at overall catalyst amounts higher than 30×10^{-3} Pd + Rh mmol (Table 6, Figure 8). However, a linear correlation was observed at lower catalyst amounts.

Finally, the catalytic activity was evaluated as a function of the relative amount of either rhodium or palladium in the catalysts, keeping H_2 pressure (30 bar) and benzene concentration (0.16 M) constant (Table 7). As is straightforwardly shown in Figures 9 and 10, a linear correlation between TOF and metal content was found for either metal, with a major slope exhibited by the rhodium graph. Quite similar results have been obtained in the hydrogenation of toluene, the only difference being that it was reduced at a slower rate than benzene, most likely due to steric effects (Table 8).[4]

Interestingly, when the zeolite-supported catalyst $Rh^{I}-Pd^{0}$/NaY (0.15−2.01 wt % Rh−Pd) was substituted for $Rh^{I}-Pd^{0}/SiO_2$ in a standard hydrogenation reaction of benzene (30 bar H_2, 40 °C, 47 mg of catalyst, 0.43 mL of benzene, 2 h, *n*-pentane), the activity (4% conversion, TOF = 11) was identical to that obtained with a pure sample of Pd^{0}/NaY under comparable experimental conditions, with no appreciable effect of the rhodium single sites. No positive effect on the conversion of benzene was similarly reported for hydrogenation reactions catalyzed by $Rh(CO)_2$(sulfos)$-Pd^{0}/SiO_2$, which differs from $Rh^{I}-Pd^{0}/SiO_2$ in having two CO co-ligands in the place of cod.[1d,4] This evidence confirms that the tethered rhodium complex must bear an easily reducible co-ligand to generate a better catalyst than Pd^{0}/SiO_2 and also rules out that the simple presence of phosphine ligands on the support may increase the catalytic activity of the Pd^{0} particles.

Benzene Hydrogenation Regiochemistry. The reduction products of C_6D_6 with H_2 in the presence of either Pd^{0}/SiO_2 or $Rh^{I}-Pd^{0}/SiO_2$ were examined by NMR spectroscopy and GC/MS. The $^{13}C\{^{1}H\}$ NMR spectrum of the product obtained with Pd^{0}/SiO_2 (Figure 11a) showed the formation of several regioisomers $C_6H_{6+x}D_{6-x}$, which is consistent with the fact that palladium particles, besides hydrogenating benzene to cyclohexane, disproportionate cyclohexa-1,3-diene to benzene and cyclohexene.[27] This means that also C−H/C−D exchange is achieved (GC/MS evidence). The major product was the cis−trans regioisomer, followed by the all-cis regioisomer (Chart 1). The $^{13}C\{^{1}H\}$ NMR spectrum of the product obtained with $Rh^{I}-Pd^{0}/SiO_2$ was quite similar except for a higher proportion of the all-cis isotopomer (Figure 11b).

The regiochemistry of benzene-d_6 hydrogenation by heterogenized single-site catalysts has been previously studied for organoactinides and organozirconium complexes.[28] In either case, mixtures of all-cis and cis−trans isotopomers were obtained, with a prevalence of the latter. In contrast, the homogeneous hydrogenation of benzene catalyzed by $(\eta^3\text{-}C_3H_5)$-$Co(PR_3)_3$ (PR_3 = phosphite, phosphine) has been found to give exclusively the all-cis product.[29] The complexed isotopomer distribution obtained with $Rh^{I}-Pd^{0}/SiO_2$ can be accounted for by the concomitant presence of the palladium nanoparticles, yet the increased proportion of the all-cis product suggests that the rhodium single sites may have a their own role, similar to that of the cobalt complex, along the hydrogenation path down to cyclohexane, once benzene is activated by palladium (see below).

Proposed Catalytic Mechanism. A number of key points have been unambiguously established in the course of the experimental studies reported in this paper, which can be summarized as follows:

(i) The much faster hydrogenation rate of $Rh^{I}-Pd^{0}/SiO_2$ as compared to Pd^{0}/SiO_2 is due not to a hydrogen spill-over effect, as suggested by some authors,[6b,g] but to the concomitant action of the two metals on the substrate. In particular, the hydrogenation of either metal and the transfer of hydrogen atoms to the substrates is not rate limiting, while both the substrate concentration and the amount of either catalyst determine the reaction rate.

(ii) The rhodium single sites must be in close contact with the palladium particles to exert a beneficial effect on the hydrogenation rate; in the absence of this requirement, as occurs for $Rh^{I}-Pd^{0}$/NaY, no rate increase is observed. In particular, there is evidence that rhodium and palladium atoms are linked to each other by a direct metal−metal bond throughout the catalytic cycle. Indirect evidence has also been obtained for the presence of hydride ligands bridging rhodium and palladium.

(iii) The ligand sulfos maintains a high degree of flexibility, even when grafted to the support, allowing the fastening/unfastening of a phosphine arm, which is certainly important for the coordination of a multi-hapto substrate.

(iv) The termination metal product after a catalysis run contains rhodium centers bonded to four carbon atoms, besides phosphorus and palladium atoms. Whether this species has the

(27) (a) Bunjes, A.; Eilks, I.; Pahlke, M.; Ralle, B. *J. Chem. Educ.* **1997**, *74*, 1323. (b) Cerveny, L.; Kluson, P.; Paseka, I. *React. Kinet. Catal. Lett.* **1991**, *43*, 533. (c) Cerveny, L.; Rehurkova, S. *Collect. Czech. Chem. Commun.* **1987**, *52*, 2909.
(28) (a) Ahn, H.; Nicholas, C. P.; Marks, T. J. *Organometallics* **2002**, *21* 1788. (b) Eisen, M. S.; Marks, T. J. *J. Am. Chem. Soc.* **1992**, *114*, 10358.
(29) Muetterties, E. L.; Rakowski, M. C.; Hirsekorn, F. J.; Larson, W. D.; Bauss, V. J.; Anet, F. A. L. *J. Am. Chem. Soc.* **1975**, *97*, 1266.

Table 6. Hydrogenation of Benzene to Cyclohexane Catalyzed by Rh^I-Pd^0/SiO_2 (0.39−9.85 wt %): Dependence on the Catalyst Amount and the Substrate Concentration[a]

entry	catalyst amount (mg)	Pd ($\times 10^3$ mmol)	Rh ($\times 10^3$ mmol)	benzene/Pd ratio	benzene/Rh ratio	benzene (mL/mmol)	yield (%);[b] TOF ($\times 10$)[c]
1	12	11.1	0.5	2015	49081	2.00/22.38	11; 12.31
2	23	21.3	0.9	1051	25607	2.00/22.38	18; 20.14
3	47	43.5	1.8	514	12531	2.00/22.38	27; 30.21
4	93	86.1	3.5	260	6333	2.00/22.38	42; 47.00
5	23	21.3	0.9	263	6402	0.50/5.59	31; 8.67
6	23	21.3	0.9	515	12548	0.98/10.97	27; 14.80
7	23	21.3	0.9	1997	48654	3.80/42.52	12; 25.51
8	23	21.3	0.9	3995	97308	7.60/85.04	6; 25.51

[a] Experimental conditions: *n*-pentane, complement to 30 mL total volume; H_2 pressure, 30 bar; temperature, 40 °C; time, 2 h; stirring rate, 1500 rpm. [b] Average values over at least three runs. [c] In mmol of product h^{-1}.

Table 7. Hydrogenation of Benzene to Cyclohexane Catalyzed by Rh^I-Pd^0/SiO_2: Dependence on Rhodium and Palladium Contents[a]

entry	catalyst	Pd content (wt %)	Rh content (wt %)	Pd ($\times 10^3$ mmol)	Rh ($\times 10^3$ mmol)	benzene/Pd ratio	benzene/Rh ratio	yield (%);[b] TOF ($\times 10$)[c]
1	Pd^0/SiO_2	1.99		8.8		547		3; 0.72
2	Rh^I/SiO_2		0.53		2.4		1688	0; 0.00
3	Rh^I-Pd^0/SiO_2	1.99	0.26	8.8	1.2	547	4052	7; 1.68
4	Rh^I-Pd^0/SiO_2	1.99	0.54	8.8	2.5	547	1951	15; 3.61
5	Rh^I-Pd^0/SiO_2	1.99	0.64	8.8	2.9	547	1646	18; 4.33
6	Rh^I-Pd^0/SiO_2	1.99	1.08	8.8	4.9	547	975	25; 6.01
7	Rh^I-Pd^0/SiO_2	1.99	1.35	8.8	6.2	547	780	33; 7.94
8	Rh^I-Pd^0/SiO_2	2.83	0.26	12.5	1.2	385	4052	10; 2.41
9	Rh^I-Pd^0/SiO_2	4.10	0.26	18.1	1.2	266	4052	13; 3.13
10	Rh^I-Pd^0/SiO_2	4.87	0.26	21.5	1.2	224	4052	16; 3.85

[a] Experimental conditions: catalyst precursor, 47 mg; benzene, 0.43 mL (4.81 mmol); *n*-pentane, complement to 30 mL total volume; H_2 pressure, 30 bar; temperature, 40 °C; time, 2 h; stirring rate, 1500 rpm. [b] Average values over at least three runs. [c] In mmol of product h^{-1}.

Table 8. Hydrogenation of Toluene to Methylcyclohexane Catalyzed by Rh^I-Pd^0/SiO_2: Dependence on Rhodium and Palladium Contents[a]

entry	catalyst	Pd content (wt %)	Rh content (wt %)	Pd ($\times 10^3$ mmol)	Rh ($\times 10^3$ mmol)	toluene/Pd ratio	toluene/Rh ratio	yield (%)[b] TOF ($\times 10$)[c]
1	Pd^0/SiO_2	1.99		8.8		534		1; 0.23
2	Rh^I/SiO_2		0.53		2.4		1688	0; 0.00
3	Rh^I-Pd^0/SiO_2	1.99	0.26	8.8	1.2	534	3953	5; 1.17
4	Rh^I-Pd^0/SiO_2	1.99	0.54	8.8	2.5	534	1903	10; 2.35
5	Rh^I-Pd^0/SiO_2	1.99	0.64	8.8	2.9	534	1606	13; 3.05
6	Rh^I-Pd^0/SiO_2	1.99	1.08	8.8	4.9	534	952	17; 3.99
7	Rh^I-Pd^0/SiO_2	1.99	1.35	8.8	6.2	534	761	23; 5.40
8	Rh^I-Pd^0/SiO_2	2.83	0.26	12.5	1.2	376	3953	8; 1.88
9	Rh^I-Pd^0/SiO_2	4.10	0.26	18.1	1.2	259	3953	11; 2.58
10	Rh^I-Pd^0/SiO_2	4.87	0.26	21.5	1.2	218	3953	13; 3.05

[a] Experimental conditions: catalyst precursor, 47 mg; toluene, 0.5 mL (4.69 mmol); *n*-pentane, complement to 30 mL total volume; H_2 pressure, 30 bar; temperature, 40 °C; time, 2 h; stirring rate, 1500 rpm. [b] Average values over at least three runs. [c] In mmol of product h^{-1}.

Figure 7. Hydrogenation reactions of benzene catalyzed by Rh^I-Pd^0/SiO_2 (Table 6, entries 2, 5−8). Dependence of the rate on benzene concentration.

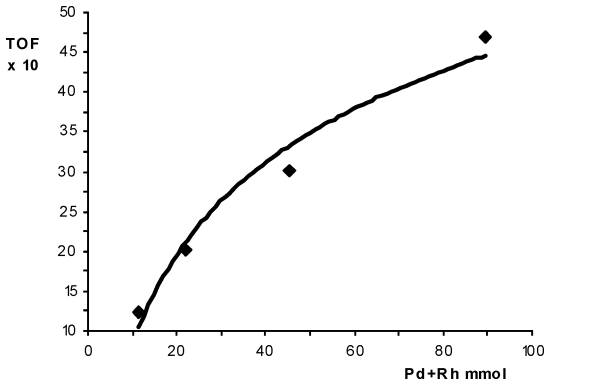

Figure 8. Hydrogenation reactions of benzene catalyzed by Rh^I-Pd^0/SiO_2 (Table 6, entries 1−4). Dependence of the rate on catalyst amount.

$\mu(\eta^4Rh\text{-}\eta^2Pd)$ benzene structure proposed in Scheme 6 is a matter of troublesome assessment. However, this is quite likely as, if it were a Rh-η^4-cylohexa-1,3-diene product, it would be very difficult to intercept due to the fast kinetics of cyclohexadiene reduction at the rhodium single site.[4] In this respect, the increased proportion of all-cis cyclohexane in the reduction of C_6D_6 with H_2 on Rh^I-Pd^0/SiO_2, as compared to Pd^0/SiO_2, is an indirect proof that, once benzene is concomitantly activated

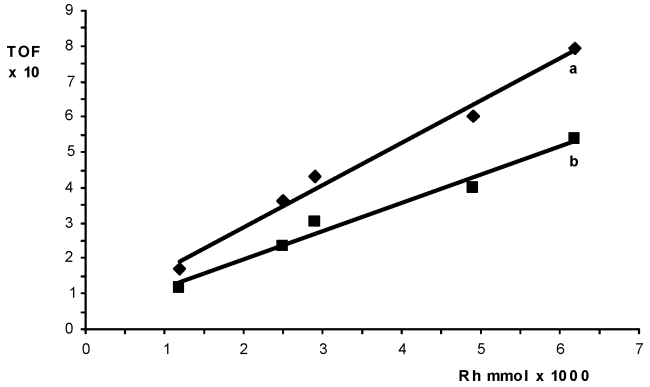

Figure 9. Hydrogenation reactions of benzene (a) and toluene (b) catalyzed by Rh^{I}–Pd^{0}/SiO_2 (Tables 7 and 8, entries 3–7). Dependence of the rate on rhodium content.

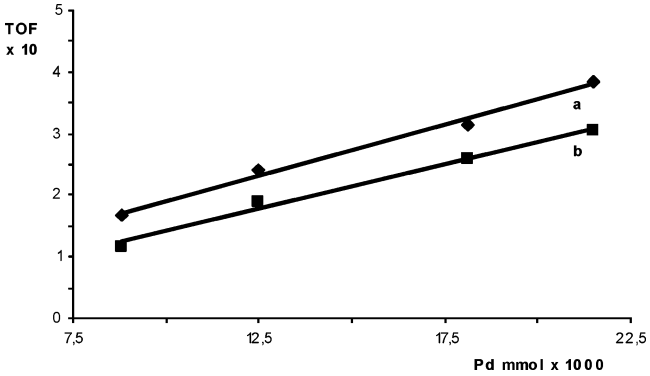

Figure 10. Hydrogenation reactions of benzene (a) and toluene (b) catalyzed by Rh^{I}–Pd^{0}/SiO_2 (Tables 7 and 8, entries 3, 8–10). Dependence of the rate on palladium content.

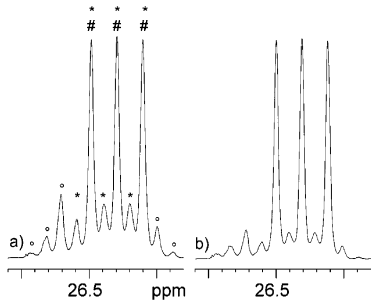

Figure 11. $^{13}C\{^{1}H\}$ NMR spectrum (21 °C, C_6D_6, 100.613 MHz) in the cyclohexane region of the mixture of products obtained by hydrogenation of C_6D_6 in the presence of (a) Pd^{0}/SiO_2 and (b) Rh^{I}–Pd^{0}/SiO_2. Representative resonances attributed to all-cis, cis-trans products and C–H/C–D exchange products are marked with #, *, and °, respectively.

Chart 1

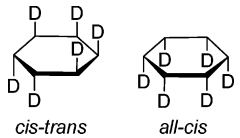

by the two metals, the rhodium single sites can then bring about by themselves the stepwise reduction by stereoselective H_2 cis additions.[20b,26,29] On the other hand, a relevant contribution to the catalysis would be still made by palladium, especially as regards the hydrogenation of cyclohexene.[4]

At this stage, it is worth commenting on a well-documented case of homogeneous hydrogenation of benzene by (η^3-C_3H_5)-$Co(PR_3)_3$ (PR_3 = phosphite, phosphine) described by Muetterties.[26] This author was able to show that the true catalyst is a Co hydride with two phosphine ligands, which coordinates benzene in the η^4-fashion, to give a transient $CoH(\eta^4\text{-}C_6H_6)(PR_3)_2$ complex, followed by intramolecular hydride transfer to give the allylic intermediate $Co(\eta^3\text{-}C_3H_7)(PR_3)_2$. Hydrogen addition has been proposed to generate an η^4-cyclohexa-1,3-diene complex that ultimately releases cyclohexane via H_2 addition/hydride migration steps (Scheme 7a).

Scheme 7

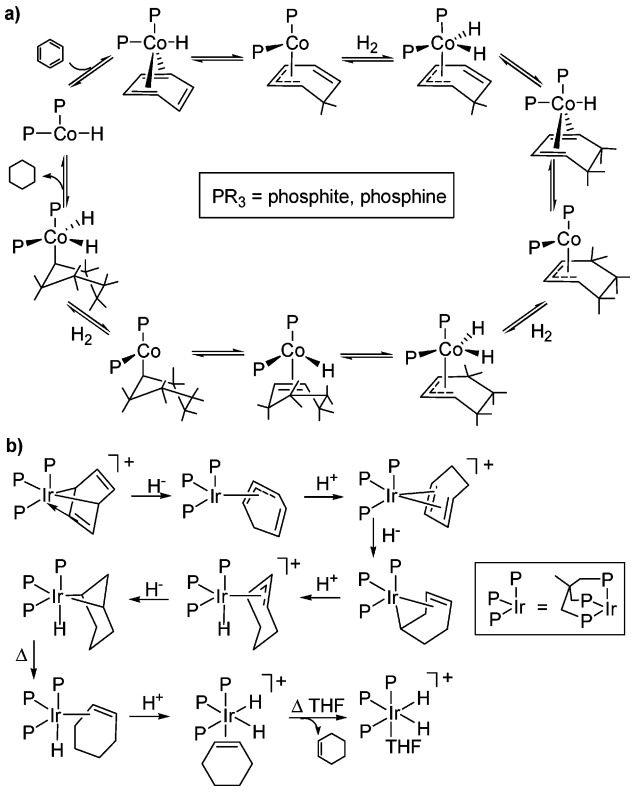

The mechanism of benzene hydrogenation demonstrated for the cobalt complex is apparently inaccessible to the "Rh^{I}(sulfos)" fragment, either free or supported, due to its inability to activate benzene in the η^4-fashion, at least within the temperature range that precedes its decomposition. Only when the benzene ligand is artificially created around the metal center, as in $[Ir(\eta^4\text{-}C_6H_6)(triphos)]^{+}$, obtained by cyclotrimerization of acetylene, has the η^4-coordination of benzene been observed for a $16e^{-}$ metal fragment.[25] However, this Ir complex is *not* a catalyst for benzene hydrogenation. Only through separate multi-additions of either H^{-} or H^{+} could the benzene ligand in $[Ir(\eta^4\text{-}C_6H_6)(triphos)]^{+}$ be selectively reduced to cyclohexene (Scheme 7b). Nevertheless, it is interesting and thought-provoking to notice that the Ir and Co catalytic cycles share most of the same intermediates, which suggests an analogous mechanism for grafted "Rh^{I}(sulfos)", which is isostructural and isoelectronic to "Ir^{I}(triphos)", provided that palladium activates the substrate and the Rh fragment.

From a comparison of the reaction sequences for Co and Ir, one may also realize that either system promotes the hydrogenation of benzene through intermediates that bear a single hydride ligand. This commonality suggests that, in the benzene hydrogenation catalyzed by Rh^{I}–Pd^{0}/SiO_2, the Pd nanoparticles may also control the number and nature of the hydride ligands at the Rh site, possibly generating more reactive monohydride

Scheme 8

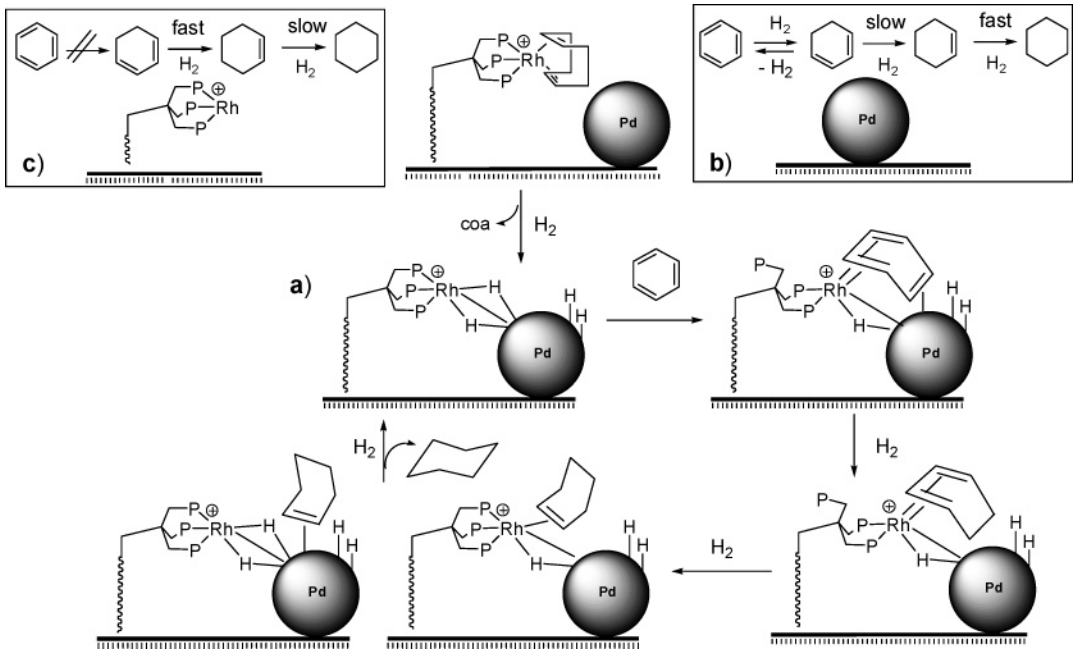

species. This reaction opportunity is well known in homogeneous hydrogenation reactions, where the dihydride systems $[Rh(H)_2(sulfos)]$, $[Rh(H)_2(triphos)]^+$, and $[Ru(H)_2(triphos)]^{2+}$ can be converted to the more active monohydride systems $[RhH(sulfos)]^-$, $[RhH(triphos)]$, and $[RuH(triphos)]^+$, respectively, by deprotonation with strong bases.[1a,20,30] In fact, the hydride migratory addition to C−C double bonds is generally easier for Rh monohydrides than for Rh dihydrides, as the latter can undergo competitive H_2 reductive elimination.

On the basis of the new experimental data described in this work, incorporated with the data previously reported and with relevant literature reports, a full mechanism for the hydrogenation of benzene by Rh^I-Pd^0/SiO_2 can therefore be proposed (Scheme 8).

The overall mechanism comprises three distinct reaction paths that reflect the concomitant presence on the support material of chemically interacting Rh^I single sites and palladium nanoparticles (a), isolated palladium nanoparticles (b), and isolated Rh^I single sites (c). The catalytic action of the latter two is well established: Pd^0 is able to reduce benzene to cyclohexane with a mechanism that involves disproportionation of the cyclohexa-1,3-diene product and fast cyclohexene hydrogenation; Rh^I is faster than Pd^0 in reducing cyclohexa-1,3-diene, yet slower in the conversion of cyclohexene to cyclohexane.[4] It is our opinion that the combined action of the two catalysts compensates for each individual weak point: upon hydrogenation of Rh^I-Pd^0/SiO_2, the Rh single site and the Pd particle form a unique, stable heterobimetallic catalyst in which Pd adsorbs and activates benzene so as to allow its η^4-coordination to Rh (favored by unfastening of a phosphine arm), followed by reduction to cyclohexa-1,3-diene. Fast hydrogenation of cyclohexa-1,3-diene (prevalently at the Rh site) would also prevent the undesired disproportionation at Pd, and the resulting cyclohexene would be hydrogenated to cyclohexane by either metal (prevalently on Pd).

Conclusions

This paper reports an in-depth study of benzene hydrogenation over a silica-supported catalyst that combines a grafted rhodium complex and palladium nanoparticles. In situ and ex situ EXAFS and DRIFT measurements, batch catalytic reactions under different conditions, deuterium labeling experiments, and model organometallic studies, taken together, have provided valuable information on the mechanism by which rhodium single sites and palladium nanoparticles cooperate with each other in promoting the hydrogenation of arenes.

The rhodium complex and the palladium particles form a unique, stable entity throughout the catalytic cycle. Besides decreasing the extent of cyclohexa-1,3-diene disproportionation at palladium, the combined action of the two metals activates the arene so as to allow the rhodium sites to enter the catalytic cycle and speed up the overall hydrogenation process by rapidly reducing benzene to cyclohexa-1,3-diene.

Acknowledgment. The LURE synchrotron laboratory in Orsay (Paris, France) and the staff of the XAS-13 beamline are gratefully acknowledged for the support and technical assistance. We also thank the Ministry of University and Research of Italy (MIUR) for financial support (FISR project: Nanotecnologie molecolari per l'immagazzinamento e la trasmissione delle informazioni) and the European Commission for financing the Network of Excellence IDECAT (contract n*o*. NMP3-CT-2005-011730).

Supporting Information Available: Syntheses of Pd^0/SiO_2 and Rh^I/SiO_2, recycling procedures of the heterogeneous catalysts, and details of acquisition of DRIFT spectra and HRTEM micrographs. This material is available free of charge via the Internet at http://pubs.acs.org.

JA060235W

(30) Bianchini, C.; Casares, J. A.; Meli, A.; Sernau, V.; Vizza, F., Sanchez-Delgado R. A. *Polyhedron* **1997**, *16*, 3099.